RSC Advances

PAPER

View Article Online
View Journal | View Issue

Cite this: *RSC Adv.*, 2023, **13**, 19235

Adsorption and desorption of flavonoids on activated carbon impregnated with different metal ions†

Li Lu, ‡[a] Shuang Cao,‡[a] Zhexuan Li,[a] Jingdan Huang,[a] Yukai Jiang,[a] Changyong Deng,[a] Zhimei Liu*[b] and Ziwei Liu*[a]

Received 24th May 2023
Accepted 6th June 2023

DOI: 10.1039/d3ra03476c

rsc.li/rsc-advances

In this study, four metal ions Mg^{2+}, Al^{3+}, Fe^{3+}, and Zn^{2+} were loaded on the surface of activated carbon by an impregnation method coupled with high-temperature calcination to prepare modified activated carbon. Scanning electron microscopy, specific surface area and pore size analysis, X-ray diffraction, and Fourier infrared spectroscopy were used to evaluate the structure and morphology of the modified activated carbon. The findings show that the modified activated carbon had a large microporous structure and high specific surface area, both of which significantly improved absorbability. This study also investigated the adsorption and desorption kinetics of the prepared activated carbon for three flavonoids with representative structures. The adsorption amounts of quercetin, luteolin, and naringenin in the blank activated carbon reached 920.24 mg g^{-1}, 837.07 mg g^{-1}, and 677.37 mg g^{-1}, while for activated carbon impregnated with Mg, the adsorption amounts reached 976.34 mg g^{-1}, 963.39 mg g^{-1}, and 817.98 mg g^{-1}, respectively; however, the desorption efficiencies of the three flavonoids varied a lot. The differences in desorption rates of naringenin as compared with quercetin and luteolin in the blank activated carbon were 40.13% and 46.22%, respectively, and the difference in desorption rates increased to 78.46% and 86.93% in the activated carbon impregnated with Al. The differences provide a basis for the application of this type of activated carbon in the selective enrichment and separation of flavonoids.

1 Introduction

Activated carbon (AC) is a kind of carbon adsorption material with a rich porous structure and huge specific surface area.[1] Commonly used powdered AC has high mechanical strength and good mechanical and chemical stability.[2] Activated carbon has a wide range of biomass sources, such as coffee husk,[3] shea residue,[4] avocado seeds[5] and straws; the biomass can also be prepared as a graphene material to catalyze the production of biodiesel from microalgae lipids under solar energy.[6] Therefore, it is widely used in adsorption, separation, catalysis, medicine and other fields.[7] In the pharmaceutical industry, AC is often used for the removal of pyrogens from purified water and air purification. AC can be used in clinical settings for the treatment of food poisoning and diarrhea; therefore, AC is considered to have good biocompatibility.[8] The adsorption capacity and performance of AC are influenced by many factors, such as raw materials, specific surface area, elemental content, surface functional groups, pore size distribution and surface charges.[9,10] The AC properties can be attributed to the elemental composition. Besides C element, AC is composed mainly of O, N, P and S elements; hetero-atoms exist mainly in the form of surface functional groups and give AC different applications.[11] The type and quantity of these elements depend either on the nature of the starting material or the chemical or physical reactions during activation.[12,13] These basic elements form the porous skeleton structure and surface carbon-bearing functional groups in AC.[14,15] Therefore, the surface chemical properties of AC can be further modified by oxidation, reduction and loading of metal ions.[16,17] Among these, metal ion modification of AC is a simple and common method with diverse application prospects.[18] During modification, reactions between AC and metal ions can form more diverse functional groups, and even generate chemical adsorption with adsorbate, finally extending the application of AC.[19] Due to the safe and low-cost nature of AC in the pharmaceutical field, metal ion modification can also be combined with other modification methods, and the modification schemes prefer metal ions with good biocompatibility.[20,21] For example, studies have shown that water vapor activation increases the specific surface area of AC mediated by Fe_3O_4. The specific surface area after steam gasification is

[a]*School of Chemical Engineering & Pharmacy, Wuhan Institute of Technology, Xiongchu Avenue, No. 693, Wuhan, China. E-mail: ziweil31@163.com*

[b]*Wuhan WUYAO Pharmaceutical Co., Ltd, Grand Pharmaceutical Co., Ltd, China Grand Enterprises Inc., Wuhan Optics Valley International Biomedical Industry Base, Gaokeyuan No. 693, Wuhan, China. E-mail: zmeileo@yeah.net*

† Electronic supplementary information (ESI) available. See DOI: https://doi.org/10.1039/d3ra03476c

‡ These authors contributed equally to this work and should be considered co-first authors.

546.91 $m^2 g^{-1}$, which is 4 times higher than that before steam gasification.[22] Thus, developing metal ion modification technologies that are easy to industrialize will be beneficial for improving the application performance of AC and enriching application scenarios.[23]

In a narrow sense, the structure of flavonoids refers to 2-phenylchromones, such as flavone and flavonol types.[24,25] For example, luteolin from the honeysuckle belongs to the flavone type, and quercetin from ginkgo belongs to the flavonol type. Besides flavone and flavonol, naringenin with a saturated C2–C3 bond on the C-ring is classified as a flavanone.[26] Many flavonoids have anti-inflammatory,[27] expectorant, cough-suppressant, calming, antifungal, and antibacterial properties.[28] Thus, the flavonoids are used as adjunctive treatments for chronic and acute hepatitis,[29,30] anti-tumor,[31,32] free radical damage[33] and oxidative stress.[34,35]

The common method for the separation and purification of flavonoids is column chromatography. Silica gel and glucan gel column chromatography are widely used in the lab for the separation of isoflavone, flavanone, flavanonol, highly methylated flavonoid and flavonol.[36] They can also be used to separate highly polar flavonoids, such as polyhydroxy flavonols and their glycosides, but the cost of silica gel and glucan gel column chromatography in industry is high. Macroporous resins and polyamide column chromatography are ideal commercial adsorbents for flavonoid enrichment.[37] Their adsorption abilities mainly come from the competitive hydrogen bonds that form between the solvent, flavonoid and adsorbent. Macroporous resins and polyamide column chromatography can be used to obtain various types of flavonoids, including glycosides and aglycones, chalcone and flavanones from extracts.[38] However, with macroporous resins and polyamides, it is difficult to achieve a fine separation effect for different flavonoids.[39] Recently, a modified AC column was developed by our group as a column packing material for saccharide purification. Research shows that eight monosaccharides, disaccharides, and trisaccharides can be separated by the columns packed with AC impregnated with zinc chloride.[40] Consequently, powdered AC was further explored by our group as a separation and purification agent for flavonoids. In this paper, we have screened different combinations of AC with four common metal ions, studied their adsorption and desorption on three typical flavonoids and explain the mechanism. The prepared AC exhibits different desorption effects on the three flavonoids, with the desorption rate of naringin exceeding 80%, and the desorption rates of luteolin and quercetin from modified AC range from 2% to 20%, providing the AC with the potential for further development as a flavonoid enrichment material.

2 Experimental

2.1 Preparation of modified active carbon

Powdered AC was sieved (300 mesh) to remove the large particles and washed with 0.1 mol L^{-1} hydrochloric acid to eliminate the soluble impurities. The AC was then dried in a drying oven at 60 °C until use. After pre-treatment, 10 g AC was stirred with 100 mL of aqueous solutions of $MgSO_4$, $AlCl_3$, $FeCl_3$ and $ZnCl_2$ at a concentration of 0.1 mol L^{-1} for 24 h. The four kinds of metal ions-impregnated AC and the blank control AC were further carbonized under N_2 protection in a tube furnace at 800 °C for 2 hours. Herein, AC was impregnated with four types of metal ions and denoted as MgAC, AlAC, FeAC, and ZnAC, respectively; AC without calcination and ion metal impregnation was denoted as BKAC, and AC with only calcination was abbreviated as CKAC. All reagents were purchased from Macklin; medicinal grade AC made from straw was obtained from J&K.

2.2 Preparation of flavonoids standard curve

Quercetin, luteolin and naringenin standards (0.1 g) were accurately weighed in a beaker and the volume was fixed with 95% ethanol in a volumetric flask to obtain 100 mg L^{-1} of flavonoid working solution. Exactly 0.0, 5.0, 10.0, 20.0, 30.0 and 40.0 mL of the flavonoid standard solution were pipetted into a 100 mL volumetric flask. The maximum absorption wavelengths detected using a UV spectrophotometer for luteolin, quercetin, and naringenin were 350 nm, 370 nm, and 288 nm. The quantitative relationship between the concentration and absorbance was plotted by measuring the absorbance at a wavelength with 95% ethanol as a reference. Linear regression was performed by the least squares method to obtain the regression equation between flavonoid concentration (Y) and absorbance (A).

2.3 The morphology and structural characterization of AC

The surface morphologies of AC dried overnight at approximately 103 °C under vacuum were characterized by scanning electron microscopy (SEM-EDS; Zeiss, EVO 50 Model), with an acceleration voltage of 0.2 to 30 kV, and a magnification of 5 to 1 000 000×. The surface functional groups of AC were determined using a Fourier Transform Infrared Spectrometer (FTIR) with a scanning wave range from 4000 to 500 cm^{-1}, resolution of 1 cm^{-1}, and scanning speed of 2 mm (TuoPu, FTIR920). X-ray diffraction (XRD) analysis was conducted on an X-ray diffraction meter (Bruker, D8 DaVinci), equipped with Cu-Kα radiation (λ = 1.5404 Å), Lynx-Eye linear position sensitive detector and Ni-filter, and an angle accuracy of 0.0001 degrees. Data was collected between $2\theta = 5°$ and 90° with a count time of 0.05 per step. The ACs were dispersed in distilled water for particle size determination using dynamic light scattering (Horiba, La-300) over a wide dynamic measurement range of 0.01–5000 microns. BET (Brunauer, Emmett, Teller) gas sorptometry was conducted to examine the specific surface area and the porous nature of AC; the analysis range of the specific surface area was 0.005 $m^2 g^{-1}$ without an upper limit, and the pore size analysis range was 3.5–500 Å. The specific surface area for AC was calculated using Langmuir and BET equations. The pore size distribution was calculated from the desorption isotherms using the Horvath–Kawazoe model, and the pore volume was calculated using the t-plot model. The above characterizations were applied to the AC before flavonoid separation.

2.4 Adsorption and desorption experiments of flavonoids on activated carbon column

In this work, the prepared AC was applied to enrich flavonoids by dynamic column elution. The modified AC powder was soaked in 95% ethanol, and the column was loaded by a wet method (column length 30 cm, diameter 1 cm). Here, 0.1 g luteolin, quercetin, and naringin were precisely weighed and dissolved in 100 mL of ethanol; 100 mL of 1 mg mL^{-1} flavonoid solution was soaked in the column to reach adsorption equilibrium, referring to the time determined by the adsorption kinetics experiment. Sodium *t*-butoxide with 95% ethanol solution (pH = 10) was applied to elute the AC column, and the flow rate was controlled at 1 mL min^{-1} by pressurization. The elution end-point was judged by a 1% $FeCl_3$ colour reaction. The flavonoid content in the eluate was quantitatively evaluated by HPLC.

2.5 Adsorption kinetics experiment

The steps for the intermittent adsorption method of static adsorption are as follows. The 0.1 g mL^{-1} 100 mL flavonoid solution was stirred with excess AC at 25 °C in a beaker to establish the adsorption equilibrium using the constant concentration of the aqueous flavonoid as the ending point. The upper aqueous phase was extracted at various time intervals before and after the establishment of adsorption balance, followed by membrane filtration to obtain the samples for UV determination. The following equation was used to compute the adsorption capacity:

$$q_e = \frac{v(c_o - c_e)}{m}$$

where q_e is the adsorption capacity at an equilibrium concentration of c_0, g g^{-1}; v is the volume of the adsorbent solution, L; c_0 is the initial mass concentration of the adsorbent in the solution, g L^{-1}, c_e is the residual mass concentration of adsorbent at AC adsorption equilibrium, g L^{-1}; m is the mass of AC sample, g.

2.6 Statistics

All data were processed at least three times. Data were analysed using the SPSS 19.0 software. The results were calculated as mean ± standard deviation (SD) and evaluated by one-way ANOVA and Dunnett *post hoc* test comparisons.

3 Results and discussion

3.1 Morphological and structural characterization of AC

The SEM images of AC before and after modification are shown in Fig. 1a–f (×1000) and Fig. S1† (×5000). The powdered AC employed in this study has a homogeneous particle size and low diffusion resistance, which underpin column elution. As shown in Fig. 1a, the huge pores of various shapes, sizes, and depths at the AC micron level can be readily seen on the surface of BKAC. Fig. 1b–f depict the morphological changes of AC subjected to calcination at 800 °C and metal ion impregnation. After calcination, as a result of large pores collapsing, the surface of AC became smoother, which reduced the resistance with elution. The steam thermal expansion and metal ion occupation effect during calcination give AC a differentiated surface appearance.

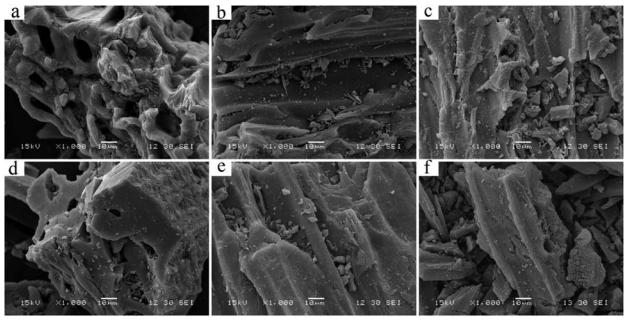

Fig. 1 SEM images of modified and unmodified AC (×1000). (a) SEM image of BKAC. (b) SEM image of CKAC. (c–f) SEM images of AC calcined and impregnated with Mg, Al, Fe, and Zn metal ions.

3.2 Surface functional groups of AC

Due to the similar chemical environments to which the functional groups on the AC surface belong, the analysis of functional groups on the AC surface often focuses on the changes in the numbers of certain types of functional groups.[41,42] In this study, calcination in a hypoxic environment typically leads to an increase in alkylation in the AC, while the reducibility of metal ions causes a decrease in the number of carbonyl groups.[43] These carbonyl groups are partially converted into hydroxyl groups, mediated by metal ions, leading to an increase in the number of hydroxyl groups in the metal ion impregnation groups.[44] The peak attribution of AC is as follows:

The stretching and bending vibrations caused by the composition difference of C, H, and O elements on the surface of different AC are described below. The strong absorption bands appearing at 3790 cm^{-1} are attributed to the increased stretching vibrations of the –OH group after high-temperature

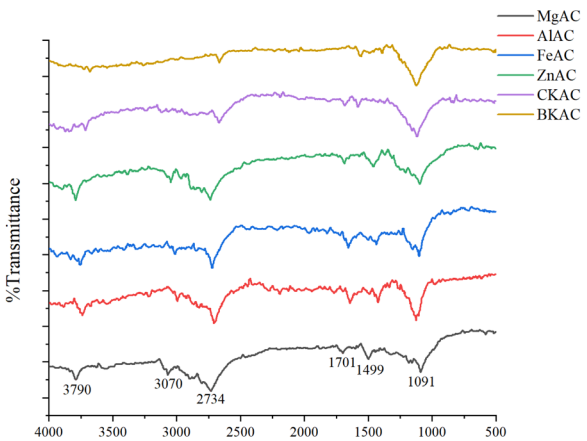

Fig. 2 FTIR spectra of the AC. From top to bottom are the spectra of the AC calcined and impregnated with Mg, Al, Fe and Zn metal ions, the spectrum of AC only with calcination, and the spectrum of AC used as blank control.

calcination;[45] the increase is particularly significant after the interaction of the AC surface and metal ions. The symmetric and asymmetric stretching vibrations of the aliphatic hydrocarbons, –CH, $–CH_2$, and $–CH_3$,[46] are responsible for the absorption peaks at 3070 and 2734 cm^{-1}. The absorption peak at 1701 cm^{-1} represents the –C=O stretching vibration of a ketone, aldehyde, lactone, or carboxyl group. The impregnated groups displayed a stronger absorption peak intensity at 1499 cm^{-1} as compared with that in the blank control. This is likely because the high-temperature calcination and the metal ions change the –C–O–C– bonds of ether functional groups on the AC surface. The absorption peak at 1091 cm^{-1} corresponds to the in-plane bending vibration of –C=O.[47] The similar peaks for the six samples indicated the consistency in the patterns of the functional groups and the differences in the functional group content (Fig. 2).

3.3 Particle size analysis of AC

The ACs with smaller particle sizes have larger specific surface areas and relatively simple void and crack structures. In the study, the large specific surface could improve the interaction probability between the adsorbate and adsorbent. The simple void and crack structure in AC powder causes the adsorbate to be easily desorbed during the elution, thus avoiding the formation of dead adsorption. The results of this experiment are presented in Fig. 3 and S2† and show that the calcined AC has a significantly smaller particle size than that in uncalcined AC, and there is no statistical difference in particle size between calcined AC only and AC calcined and impregnated with metal ions. The results further demonstrated that calcination has a significant effect on the particle size of AC, and metal ion impregnation has no obvious effect on the particle size of AC. Moreover, the particle size distribution in all groups could be fitted to the normal distribution with a small deviation. The homogeneity of AC particles ensures stability and reproducibility in a column elution process.

3.4 Specific surface area and pore size distribution of AC

The amount of gas that AC adsorbs in a sealed system at a given temperature corresponds precisely to the pressure at which adsorption equilibrium is reached.[48] The isotherms of all AC investigated in this experiment are classified as IUPAC type IV isotherms. The type IV isotherm is distinguished by the slender hysteresis loop between the adsorption and desorption curves. As shown in Fig. 4 and S3,† when $p/p^0 < 0.1$, the one-layer nitrogen adsorption occurs on the surface of micropores in the AC, and the efficient and rapid adsorption behaviour confirmed the presence of a large number of micropores in AC. When $p/p^0 > 0.1$, the adsorption capacity of AC increases as the relative pressure rises, but the rate of increase is significantly slowed down as compared with the low-pressure adsorption zone. The decrease in the adsorption rate confirmed that multilayer adsorption occurred in macropores and mesopores. When $p/p^0 = 0.5$, the phenomena of trailing and hysteresis loops appeared in all groups, caused by capillary condensation that occurs in the macropores and mesopores of AC. When $p/p^0 = 0.9$, multilayer adsorption takes place in the AC, and capillary coalescence occurs at higher partial pressures. Therefore, the adsorption capacity increases significantly in this pressure range. Although the six kinds of AC show similar type IV isotherms, their rising curves in the low-pressure zone and the values of the maximum adsorption capacity have led to the following conclusions. The N_2 adsorption capacity of the calcined AC is much higher than that of the uncalcined AC, and there is no obvious difference between the calcined AC impregnated with different metal ions. After calcination, the enlargement of existing pore channels and the generation of new pore channels in AC due to the thermal expansion effect caused an increase in micropores. Moreover, the metal ions interacting with some components on the surface of AC not only form new functional groups that are favourable for adsorption but also increase the total adsorption capacity to varying degrees.

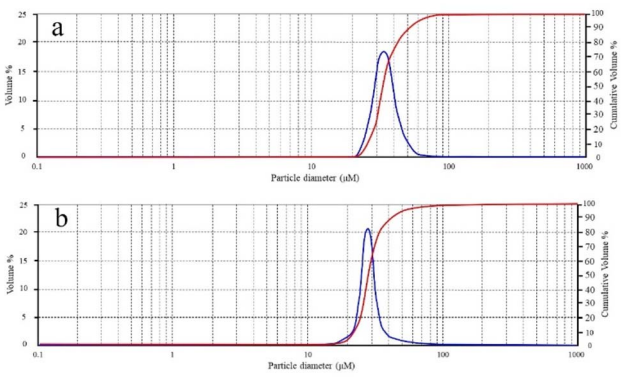

Fig. 3 Particle size analysis figures of activated carbon. (a) The particle size analysis of blank activated carbon (BKAC) without any treatment. (b) The particle size analysis of calcined activated carbon (CKAC).

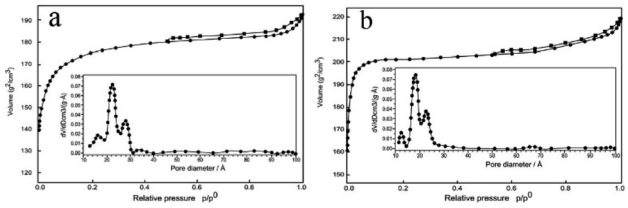

Fig. 4 BET analysis and pore size distribution. (a) The pore size distribution of activated carbon (BKAC) without any treatment, and (b) the calcined activated carbon (CKAC).

3.5 Energy dispersive spectroscopy analysis of AC

The changes in the amounts of primary elements in AC after the modification are shown in Fig. 5. The impregnation concentrations allow metal ion excess as compared to the adsorption amount of the AC, which is determined by the metal ion concentration in the impregnation supernatant. Generally speaking, more oxygen on the surface of AC will result in more cation exchange properties of AC, which is conducive to adsorbing polar substances; conversely, less oxygen on the surface of AC will result in more anion exchange properties,

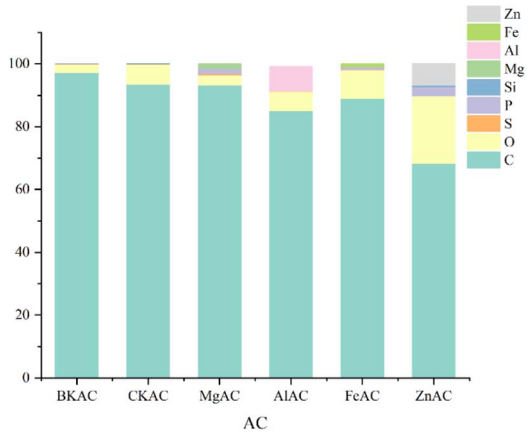

Fig. 5 Surface elements of modified AC were analysed by EDS.

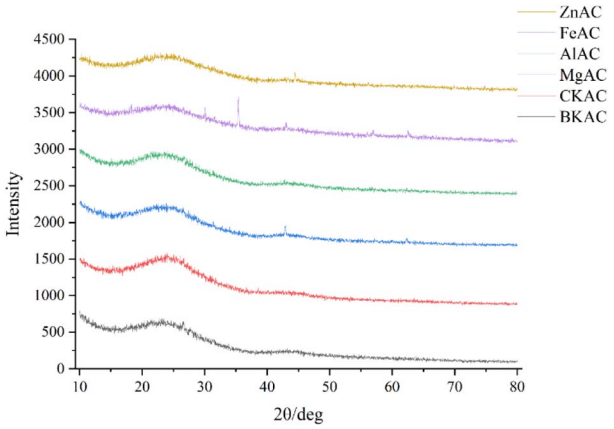

Fig. 6 The XRD analysis of AC.

which is conducive to adsorbing non-polar substances.[49] Fig. 5 shows that uncalcined AC was comprised mainly of C and O with trace amounts of P and S. Compared with the AC impregnated with metal ions, the BKAC and CKAC have lower oxygen content, making them more suitable for the adsorption of less polar or non-polar chemicals. In the impregnation groups, Mg^{2+}, Al^{3+} and Fe^{3+} are considered hard acids under the theory of hard and soft acids and bases (HSAB),[50] and Zn^{2+} is considered a junctional acid. The MgAC, AlAC, FeAC, and ZnAC are more suited to the adsorption of polar compounds as compared with AC without metal impregnation. The surface acidity of AC could be increased by loading hard acid ions; this forms the specific adsorption characteristics of AC for adsorbents, which leads to firm adsorption, and the adsorbate can be desorbed under alkaline conditions.[51] The surface acidity of AC could also be increased by the loading of junctional acid ions; this forms the relatively broad adsorption characteristics of AC for adsorbents, leading to firm adsorption and difficult desorption.

3.6 XRD analysis of AC

The X-ray patterns for all AC in this study, as seen in Fig. 6, show poor crystallinity and a broad diffraction peak at $2\theta = 23$, showing the existence of a significant number of microcrystals with a disordered graphite structure in AC, primarily in the amorphous form. It is a common phenomenon that the crystallinity of carbon materials remains unchanged and the crystallite lattice changes during the modification, such as in the evolution of coal. As shown in Fig. 6, the lattice changed in the different AC groups. According to the peaks on the crystal plane, there are certain changes in the XRD patterns of AC impregnated with different metal ions. Some diffraction peaks ($2\theta =$ 31, 36, 43, 57, 62) arise for AC loaded with Fe^{3+}, which could be attributed to the divalent and trivalent Fe oxides generated by the reaction of Fe and water at high temperatures.[52] AC loaded with Mg^{2+} also generated two diffraction peaks at $2\theta = 43$, 63, followed by AC loaded with Zn^{2+} showing one diffraction peak at $2\theta = 45$. The remaining XRD patterns have no significant diffraction peaks.

3.7 Adsorption–desorption study of flavonoids on the AC column

The adsorption mechanism of AC is generally considered reversible physical adsorption for most substances. The adsorption of flavonoids by AC is more likely to occur under acidic conditions, as flavonoids containing hydroxyphenyl structures exhibit weak acidity and exist in the molecular form under acidic conditions, and the molecular form fits the characteristics of non-polar adsorption of AC.[53] For the objective of cost control and product stability, 95% ethanol was employed as the solvent for static adsorption in this experiment. Subsequently, a mixed solution of organic base and ethanol with a pH of 10 based on the pK_a of flavonoids was used as the eluent for desorption. During the elution, the flavonoid adsorbed on the AC was converted into an ionic state, and the oxygen atoms on the hydroxyl of the flavonoids were exposed in the ionic state from hydrogen bonding with the eluent. Moreover, in this ionic state, flavonoids lose their ability to interact with acidic oxygen-containing groups on activated carbon, so that the adsorbed flavonoids can be eluted.

The outcomes displayed in Fig. 7 demonstrate that each AC has potent adsorption effects for the three flavonoids with an adsorption rate of over 90%. The rich porous structure of AC and the complex forces between the flavonoids and the functional groups can cause firm adsorption. However, the flavonoids turn into ionic forms under alkaline conditions, greatly weakening their adsorption on AC, so the adsorbed flavonoids

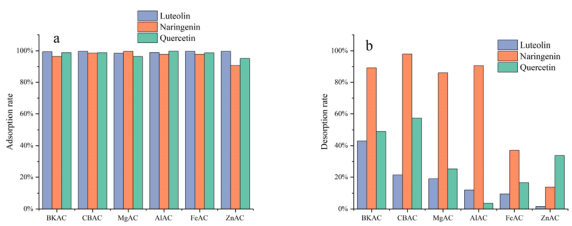

Fig. 7 Adsorption and desorption of flavonoids on AC. (a) The adsorption rates of the three flavonoids on the AC in a column, and (b) the desorption rates of the three flavonoids from the activated carbon under alkaline conditions.

can be eluted by using alkaline organic solvents. As shown in Fig. 7b, the desorption rates of the three flavonoids varied a lot. The rate of desorption of naringenin can exceed 80% under alkaline conditions; the high desorption rate of naringenin is attributed to the low abundance of hydroxyl groups. The desorption rates of luteolin and quercetin from the modified AC column are in the range of 2–20%. The desorption rates of the three typical flavonoids are higher in the AC impregnated with Mg^{2+} and Al^{3+} as compared to the AC impregnated with Fe^{2+} and Zn^{2+}, which could be because Fe^{2+} and Zn^{2+} are hard acids that have high valences and larger atomic radii in the soft and hard acid–base theory. In the presence of a large number of oxygen-containing acidic groups on the AC surface, the contribution of resonance π-electrons to AC alkalinity is masked. Therefore, increasing the alkalinity of the eluent is a method of neutralizing the acidic functional groups on the surface of AC, thereby reducing the AC adsorption for the adsorbents. Due to the presence of C-ring double bonds, the degree of dissociation of naringenin under alkaline elution conditions is stronger than that of the other two flavonoids, so naringenin can be easier eluted under alkaline solutions.[54] The impregnation of metal ions results in significant differences in the adsorption capacity of AC for flavonoids. The adsorption and desorption systems can facilitate the separation application of AC for the above three typical flavonoids.

3.8 Determination of adsorption equilibrium time

The quasi-primary adsorption rate equation, quasi-secondary adsorption rate equation, and intra-particle diffusion rate equation were used to fit the adsorption behaviour of flavonoids on AC. The quasi-secondary equation was used to predict the equilibrium adsorption amount in order to investigate the fast adsorption on the AC surface relative to the contact time.

The quasi-level model uses the Lagergren equation to calculate the adsorption rate:[55]

$$\lg(q_e - q_t) = \lg q_e - \frac{k_1 t}{2.303}$$

where q_t and q_e are, respectively, the adsorption quantities at time t and equilibrium, mg g^{-1}; k_1 is the quasi-first-order adsorption rate constant, min^{-1}.

The quasi-secondary model is described using the Mckay equation:[56]

$$\frac{t}{q_t} = \frac{1}{k_2 q_e^2} + \frac{1}{q_e} t$$

where k_2 is the quasi-secondary adsorption rate constant, g (g min)$^{-1}$.

The intraparticle diffusion model is based on the model proposed by Weber,[57] with the expression

$$q_t = k_p t^{0.5}$$

where k_2 is the quasi-secondary adsorption rate constant, mg (g $min^{0.5}$)$^{-1}$.

In this experiment, the adsorption equilibrium time and adsorption amount of quercetin, luteolin and naringenin on the prepared AC were studied under the same conditions. As shown in Fig. 8a–f, the adsorption capacity of AC after calcination was generally higher than those without calcination; this result is highly consistent with the conclusion about the increase in the specific surface area of AC in the characterization section. The flavonoids have a crossed conjugate system across the three rings with polyhydroxy properties,[58] thus the increasing OH groups on AC generated during calcination further improved the binding activities between AC and the flavonoids. However, among all groups after calcination, the adsorption capacity of AC on flavonoids showed no significant change trend. After loading metal ions, the physical adsorption sites on the surface of AC were masked but the selective coordination binding contributed by metal ions increased. This coordination and binding ability are highly related to the type of metal ions. Therefore, the adsorption capacity of MgAC for the flavonoids was greater than that of CKAC, while the adsorption capacities of the AC treated with other metal ions for the flavonoids were even lower than that of CKAC.

We further analysed Fig. 8a–f to determine the adsorption mechanism between the different modified AC and the flavonoids. As shown in Fig. 8a–c, the adsorption equilibrium times of quercetin, luteolin, naringenin and in BKAC were 20 minutes, 18 minutes, and 20 minutes, and the adsorption amount reached 920.24 mg g^{-1}, 837.07 mg g^{-1}, and 677.37 mg g^{-1}, respectively. The equilibrium times of all three flavonoids in the modified AC were similar, but the structural differences in the compounds resulted in different adsorption amounts in

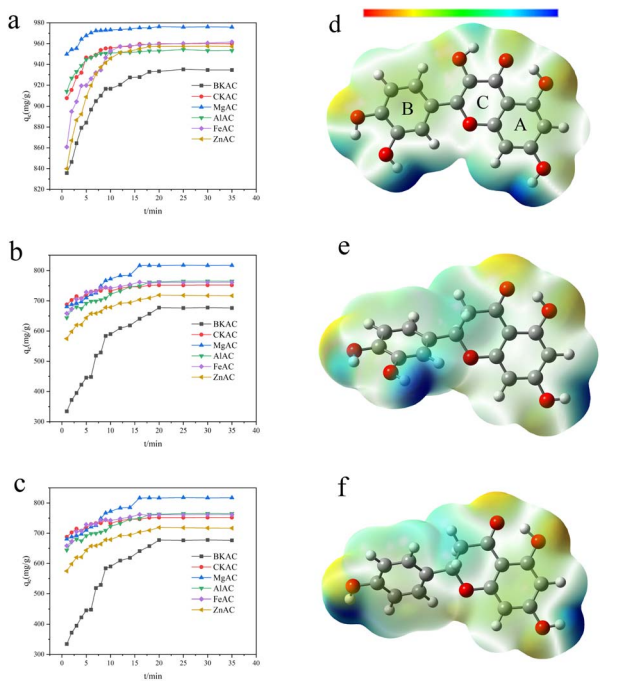

Fig. 8 The adsorption kinetics curves of six AC samples for three different flavonoids, and the electrostatic potential energies. (a–c) The adsorption curves of quercetin, luteolin and naringenin on the modified AC. (d–f) The electrostatic potential energies of quercetin, luteolin and naringenin.

AC. As shown in Fig. 8d–f, the spatial electric field density and the number of hydrogen bonds together form a differential binding force between the adsorbent and adsorbate. The adsorption capacities of flavonoid (luteolin) and flavonol (quercetin) are greater than that of flavanone (naringenin). In the study, the molecular force field analysis was applied to simulate the surface electron clouds on the three flavonoids (Fig. 8d–f). The red region in Fig. 8 has a negative electrostatic potential value, indicating that this region gives electrons easily, or is more nucleophilic as compared with other regions, while the blue region has a positive electrostatic potential value, indicating that this region gains electrons more easily and is more electrophilic. Electron transfer causes the surfaces of compounds to be distributed with electron clouds of different densities. Thus, the flavonoids can interact with the adsorbate and solvent, resulting in a difference in adsorption capacity. More specifically, as shown in Fig. 8f, the two hydrogen atoms at the C4 position on the C-ring of naringenin not only fail to contribute to the hydrogen bond binding force but also generate steric hindrance to a certain extent. Therefore, the adsorption capacity of naringenin is the lowest among the three flavonoids, thus making it easier to be desorbed in the elution. By comparing quercetin (Fig. 8d) with luteolin (Fig. 8e), quercetin has a more planar structure and is more likely to form hydrogen bond forces on the carbon plane. Therefore, AC has a higher adsorption capacity for quercetin.

4 Conclusions

In this work, the structure and surface functional groups of AC impregnated with metal ions under calcination conditions were studied. Then, the dynamic desorption and static adsorption processes of the prepared AC for three typical flavonoids were systematically studied and the adsorption kinetics were established. The study confirmed that the prepared AC had consistently high adsorption and differential desorption capacities for three typical flavonoids, the elution rate under alkaline conditions was up to 80% for naringenin, while the elution rates remained at low levels for quercetin and luteolin. The alkaline environment mediated the transformation of flavonoids into stable ionic states in the eluate, and the ionic state contributed to the differences in the interaction forces between flavonoids and AC. Considering that the structures of these three flavonoids are highly representative, the study established a new application for modified AC as a column-packing adsorbent to enrich and separate flavonoids. We also considered that the low micro homogeneity of the AC structure limits its application in fine separation. Therefore, subsequent research not only needs to constrain the structural characteristics of AC by comprehensive characterization but also needs to explore the production and preparation processes of AC to allow it to have better and more stable performances in separation applications.

Author contributions

Li Lu: conceptualization, methodology, validation, writing-original draft. Ziwei Liu: conceptualization, supervision, writing-review & editing, Shuang Cao: resources, data curation. Zhimei Liu: resources, funding acquisition, project administration. Zhexuan Li: data curation. Jingdan Huang and Yukai Jiang: investigation, validation. Changyong Deng: software.

Conflicts of interest

There are no conflicts to declare.

Acknowledgements

The authors gratefully acknowledge financial support from the innovation and entrepreneurship project of Hubei province (20201049001), and the young talent grant of Wuhan Institute of Technology (237114).

References

1 J. M. Planeix, N. Coustel, B. Coq, V. Brotons, P. S. Kumbhar, R. Dutartre, P. Geneste, P. Bernier and P. M. Ajayan, *J. Am. Chem. Soc.*, 1994, **116**, 7935–7936.
2 L. Kovalova, D. R. U. Knappe, K. Lehnberg, C. Kazner and J. Hollender, *Environ. Sci. Pollut. Res.*, 2013, **20**, 3607–3615.
3 A. M. S. Ngueabouo, R. F. T. Tagne, D. R. T. Tchuifon, C. G. Fotsop, A. K. Tamo and S. G. Anagho, *Mater. Adv.*, 2022, **3**, 8361–8374.
4 A. L. Amola, K. Theophile, T. R. Fregue, T. Tagne, C. Atemkeng, I.-H. Kuete and S. Anagho, *J. Chem.*, 2022, **2022**, 1–15.
5 T. T. R. Fregue, I. Ionel, A. S. Gabche and A.-C. Mihaiuti, *Rev. Chim.*, 2019, **70**, 410–416.
6 J. Huang, J. Wang, Z. Huang, T. Liu and H. Li, *Bioresour. Technol.*, 2023, **369**, 128390.
7 S. Gur-Reznik, I. Katz and C. G. Dosoretz, *Water Res.*, 2008, **42**, 1595–1605.
8 S. Moosavi, C. W. Lai, S. Gan, G. Zamiri, O. Akbarzadeh Pivehzhani and M. R. Johan, *ACS Omega*, 2020, **5**, 20684–20697.
9 J. Jaramillo, P. Modesto Alvarez and V. Gomez-Serrano, *Fuel Process. Technol.*, 2010, **91**, 1768–1775.
10 B. Li, Z. Lei and Z. Huang, *Chem. Eng. Technol.*, 2009, **32**, 763–770.
11 F. Zhang, Y. Tao, S. Chen and Y. Lu, *Fibers Polym.*, 2015, **16**, 2003–2010.
12 V. L. Snoeyink and W. J. Weber, in *Progress in Surface and Membrane Science*, ed. J. F. Danielli, M. D. Rosenberg and D. A. Cadenhead, Elsevier, 1972, vol. 5, pp. 63–119.
13 I. I. Salame II and T. J. Bandosz, *J. Colloid Interface Sci.*, 1999, **210**, 367–374.
14 O. V. Zabneva, S. K. Smolin, N. A. Klimenko, O. G. Shvidenko, S. V. Grechanik and A. V. Sinel'nikova, *J. Water Chem. Technol.*, 2012, **34**, 264–270.
15 K. László and A. Szűcs, *Carbon*, 2001, **39**, 1945–1953.
16 H.-L. Chiang, C. P. Huang and P. C. Chiang, *Chemosphere*, 2002, **47**, 257–265.
17 J. Yang, F. Fang and J. Zhou, *Chin. Sci. Bull.*, 2013, **58**, 3715–3720.

18 W. M. Qiao, Y. Song, S. H. Yoon, Y. Korai, I. Mochida and O. Katou, *Carbon*, 2005, **43**, 2022–2025.
19 T. J. Bandosz, *J. Colloid Interface Sci.*, 2002, **246**, 1–20.
20 A. K. Rakishev, M. D. Vedenyapina, S. A. Kulaishin and D. V. Kurilov, *Solid Fuel Chem.*, 2021, **55**, 117–122.
21 J. Rivera-Utrilla, G. Prados-Joya, M. Sanchez-Polo, M. A. Ferro-Garcia and I. Bautista-Toledo, *J. Hazard. Mater.*, 2009, **170**, 298–305.
22 T. Han, W. Yang and P. G. Jonsson, *Chem. Eng. J.*, 2020, **394**, 124902.
23 K. Chen, Z. J. He, Z. H. Liu, A. J. Ragauskas, B. Z. Li and Y. J. Yuan, *ChemSusChem*, 2022, **15**, e202201284.
24 N. Shen, T. F. Wang, Q. Gan, S. Liu, L. Wang and B. Jin, *Food Chem.*, 2022, **383**, 132531.
25 A. Garcia-Lafuente, E. Guillamon, A. Villares, M. A. Rostagno and J. Alfredo Martinez, *Inflammation Res.*, 2009, **58**, 537–552.
26 A. C. Rana and B. Gulliya, *Indian J. Pharm. Educ. Res.*, 2019, **53**, 8–20.
27 M.-H. Pan, C.-S. Lai and C.-T. Ho, *Food Funct.*, 2010, **1**, 15–31.
28 L. A. Savi, T. Caon, A. P. de Oliveira, A. M. Sobottka, W. Werner, F. H. Reginatto, E. P. Schenkel, C. R. Monte Barardi and C. M. Oliveira Simoes, *Fitoterapia*, 2010, **81**, 1142–1146.
29 J. Xiao, T. S. Muzashvili and M. I. Georgiev, *Biotechnol. Adv.*, 2014, **32**, 1145–1156.
30 G. Agati, E. Azzarello, S. Pollastri and M. Tattini, *Plant Sci.*, 2012, **196**, 67–76.
31 C. M. Passreiter, A.-K. Suckow-Schnitker, A. Kulawik, J. Addae-Kyereme, C. W. Wright and W. Waetjen, *Phytochemistry*, 2015, **117**, 237–244.
32 D. Raffa, B. Maggio, M. V. Raimondi, F. Plescia and G. Daidone, *Eur. J. Med. Chem.*, 2017, **142**, 213–228.
33 T.-y. Gao, X. Jin, W.-z. Tang, X.-j. Wang and Y.-x. Zhao, *Bioorg. Med. Chem. Lett.*, 2015, **25**, 3686–3689.
34 D. Prochazkova, I. Bousova and N. Wilhelmova, *Fitoterapia*, 2011, **82**, 513–523.
35 J. Viskupicova, M. Ondrejovic and E. Sturdik, *J. Food. Nutr. Res.*, 2008, **47**, 151–162.
36 H. J. Li, Y. Liu, Y. T. Yi, Q. Miao, S. J. Liu, F. Zhao, W. Cong, C. H. Wang and C. H. Xia, *J. Chromatogr. B: Anal. Technol. Biomed. Life Sci.*, 2017, **1048**, 56–63.
37 V. Vukics, A. Kery, G. K. Bonn and A. Guttman, *Anal. Bioanal. Chem.*, 2008, **390**, 1917–1925.
38 T. J. Mabry, K. R. Markham and M. B. Thomas, in *The Systematic Identification of Flavonoids*, Springer Berlin Heidelberg, Berlin, Heidelberg, 1970, pp. 16–22, DOI: 10.1007/978-3-642-88458-0_2.
39 H. Deka and M. D. Saikia, *Colloids Surf., A*, 2015, **469**, 51–59.
40 Z. Liu, X. Zhou, F. Wu and Z. Liu, *ACS Omega*, 2020, **5**, 10106–10114.
41 C. Moreno-Castilla, *Carbon*, 2004, **42**, 83–94.
42 P. Davini, *Carbon*, 1990, **28**, 565–571.
43 M. Polovina, B. Babić, B. Kaluderović and A. Dekanski, *Carbon*, 1997, **35**, 1047–1052.
44 L. Lavielle and J. Schultz, *Langmuir*, 1991, **7**, 978–981.
45 M. Galhetas, M. A. Andrade, A. S. Mestre, E. Kangni-foli, M. J. Villa de Brito, M. L. Pinto, H. Lopes and A. P. Carvalho, *Phys. Chem. Chem. Phys.*, 2015, **17**, 12340–12349.
46 F. Wang, X. Wang, P. Ning, X. Jing, Y. Ma, P. Wang and W. Chen, *Adsorption*, 2015, **21**, 401–408.
47 M. L. Lehmann, R. M. Counce, R. W. Counce, J. S. Watson, N. Labbe and J. Tao, *ACS Sustainable Chem. Eng.*, 2018, **6**, 374–379.
48 S. Brunauer, P. H. Emmett and E. Teller, *J. Am. Chem. Soc.*, 1938, **60**, 309–319.
49 S. X. Liu, X. Chen and X. Q. Zhang, *Environ. Sci.*, 2008, **29**, 1192–1196.
50 R. M. Lopachin, T. Gavin, A. Decaprio and D. S. Barber, *Chem. Res. Toxicol.*, 2012, **25**, 239–251.
51 A. Z. Alshemary, E. A. Pazarçeviren, A. D. Dalgic, A. Tezcaner, D. Keskin and Z. Evis, *Mat. Sci. Eng. C*, 2019, **104**, 109884.
52 H. Tian, J. Li, Q. Shen, H. Wang, Z. Hao, L. Zou and Q. Hu, *J. Hazard. Mater.*, 2009, **171**, 459–464.
53 L. Zhang, X. Zhang, Q. Li, W. Xiao, E. Su, F. Cao and L. Zhao, *ACS Omega*, 2021, **6**, 35002–35013.
54 M. S. Shafeeyan, W. M. A. W. Daud, A. Houshmand and A. Shamiri, *J. Anal. Appl. Pyrolysis*, 2010, **89**, 143–151.
55 A. Zümriye, *Biochem. Eng. J.*, 2001, **7**, 79–84.
56 G. Mckay and Y. S. Ho, *Process Biochem.*, 1999, **34**, 451–465.
57 W. J. Weber and J. C. Morris, *Oxford,* 1962, **2**, pp. 231-262.
58 B. Pahari, S. Chakraborty, S. Chaudhuri, B. Sengupta and P. K. Sengupta, *Chem. Phys. Lipids*, 2012, **165**, 488–496.